Lawrence Berkeley National Laboratory

Title
Sub-microradian Surface Slope Metrology with the ALS Developmental Long Trace Profiler

Permalink
https://escholarship.org/uc/item/0ff485z4

Author
Yashchuk, Valeriy V

Publication Date
2010-01-05

Peer reviewed

Sub-microradian Surface Slope Metrology with the ALS Developmental Long Trace Profiler

Valeriy V. Yashchuk,[a] Samuel Barber,[a] Edward E. Domning,[a] Jonathan L. Kirschman,[a] Gregory Y. Morrison,[a] Brian V. Smith,[a]

[a] *Lawrence Berkeley National Laboratory, One Cyclotron Road, Berkeley, California 94720, USA*

Frank Siewert,[b] Thomas Zeschke,[b]

[b] *Helmholtz Zentrum Berlin für Materialien und Energie, Elektronenspeicherring BESSY-II, Albert-Einstein-Str. 15, 12489 Berlin, Germany*

Ralf Geckeler,[c] Andreas Just [c]

[c] *Physikalische-Technische Bundesanstalt Braunschweig (PTB), Bundesallee 100, 38116 Braunschweig, Germany*

* E-mail: vvyashchuk@lbl.gov; Phone: +1-510-495-2592; Fax: +1-510-486-7696

ABSTRACT

A new low budget slope measuring instrument, the Developmental Long Trace Profiler (DLTP), was recently brought to operation at the ALS Optical Metrology Laboratory. The design, instrumental control and data acquisition system, initial alignment and calibration procedures, as well as the developed experimental precautions and procedures are described in detail. The capability of the DLTP to achieve sub-microradian surface slope metrology is verified via cross-comparison measurements with other high performance slope measuring instruments when measuring the same high quality test optics. The directions of future work to develop a surface slope measuring profiler with nano-radian performance are also discussed.

Keywords: x-ray optics, surface metrology, surface slope measurement, long trace profiler, LTP, surface profilometer, autocollimator, pentaprism

1. Introduction

Development of X-ray optics for 3rd and 4th generation X-ray light sources with a level of surface slope precision of 0.1-0.2 µrad requires the development of adequate fabrication technologies and dedicated metrology instrumentation and methods [1,2].

The best performing slope measuring profilers, such as the Nanometer Optical Component Measuring Machine (NOM) at Helmholtz Zentrum Berlin (HZB)/BESSY-II (Germany) [3-6] and the Extended Shear Angle Difference (ESAD) instrument at the PTB (Germany) [7-9], come close to the required precision. These instruments utilize a schematic (Fig. 1) with a movable pentaprism [10-14] and an electronic autocollimator (AC) as a contactless optical slope sensor [3,15]. The high performance of the instruments is based on the precision calibration of the ACs for the specific application with small apertures of 2.5 - 5 mm in diameter [16,17].

The Developmental Long Trace Profiler (DLTP) is a slope measuring instrument recently brought into operation at the Advanced Light Source (ALS) Optical Metrology Laboratory (OML). Similar to the NOM and ESAD, the DLTP is based on a movable pentaprism and a precisely calibrated autocollimator. In contrast to the NOM, this is a reasonably low budget instrument used at the ALS OML for the development and testing of new measuring techniques and methods. Some of the methods developed with the DLTP [18-21] have been already implemented into the ALS LTP-II slope measuring long trace profiler [22]. In the course of the developmental work, the ALS LTP-II was upgraded and has demonstrated a

1 capability for <0.25 µrad surface metrology with significantly curved optics and about
2 0.1 µrad accuracy with close to flat optics [23].

3 Besides the application as a test facility at the OML, the DLTP is developed as a slope
4 measuring instrument, supplementary to the existing LTP-II. There are a number of
5 arguments for the development. First, the systematic errors of an autocollimator-based
6 instrument should be significantly different [24] than that of the LTP [18,23]. In the LTP,
7 the optical reference arm was added [22] to monitor the carriage wiggling and laser pointing
8 instability. Unfortunately, currently, the performance of the reference arm is one of the most
9 important factors limiting the accuracy of LTP measurements [23]. The use of a movable
10 pentaprism in the DLTP makes the slope measurement insensitive, in first approximation, to
11 carriage wiggling [25], allowing for a schematic free of an optical reference arm. Second,
12 the use of an autocollimator precisely calibrated with a high performance stationary
13 calibration system, as the one at the PTB [16,17], allows transfer of calibration accuracy to
14 the DLTP measurement. Third, the closed and self-sufficient design and high stability of the
15 DLTP autocollimator [26] provides an opportunity for a deep automation of the
16 measurement process that can require very long time for efficient suppression of the errors
17 due to instrumental drifts and systematic effects.

18 In the present work, we describe the DLTP design and its major components (Sec. 2), the
19 methods used to precisely align the components (Sec. 3), and the measurement procedures
20 developed to decrease errors of the DLTP measurements (Sec. 4). In Sec. 5, the
21 performance of the DLTP is verified via a number of measurements with high quality
22 mirrors. A comparison with the corresponding results obtained with the world's best slope
23 measuring instrument, the HZB/BESSY-II NOM, as well as with the upgraded ALS LTP-II,
24 proves the accuracy of the DLTP measurements on the level of 0.1-0.4 µrad, depending on
25 the curvature of a surface under test (SUT). The directions of future work to develop a
26 surface slope measuring profiler with a reliable accuracy of <0.1 µrad are discussed in
27 Sec. 6.

28 **2. DLTP experimental set-up**

29 Figure 1 shows a simplified model of an autocollimator-based profiler. To a large extent, the
30 model depicts the arrangement and essential components of the ALS DLTP.

31
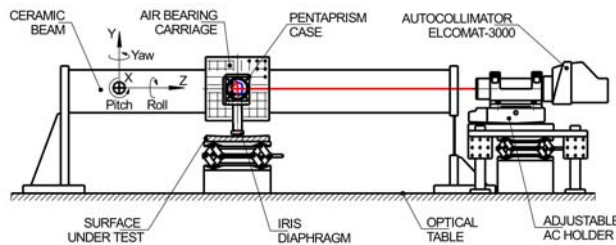
32   Figure 1: Simplified model of an autocollimator-based profiler.

33

34 The DLTP components are mounted on a Newport optical table with inactivated pneumatic
35 isolation. The complete setup is enclosed within a hutch to enable more stable (than that in
36 the laboratory) environmental conditions during a measurement. The DLTP uses an
37 electronic autocollimator "ELCOMAT 3000 special" [26] as a slope measuring optical
38 sensor. The autocollimator is mounted on a kinematic stage that allows precise alignment of
39 the autocollimator's optical axis and the direction of the carriage translation. For diverting
40 the autocollimator's light beam by 90 degrees towards the surface under test (SUT) and the
41 reflected beam back to the autocollimator, a bulk pentaprism is mounted on a Thorlabs
42 kinematic cage cube platform and placed in a cube case attached to an air-bearing carriage.

1 The carriage is translated along a ceramic beam with a Nanomotion^{TM} motor to trace the
2 surface under test (SUT) oriented face-up. Below we describe in more detail each DLTP
3 component.

2.1. Autocollimator calibrated at the PTB

5 The autocollimator ELCOMAT 3000 [26] used in the DLTP is a model originally
6 customized to work with a small aperture in the HZB/BESSY-II NOM [4]. At the specified
7 accuracy of ±0.25 arcsec (for an aperture of ≥ 5 mm), the specified instrument
8 reproducibility is 0.05 arcsec (0.24 µrad) over the total slope range of ±4.8 mrad. The high
9 reproducibility allows to increase the accuracy by applying a precise calibration and,
10 therefore, to use the autocollimator as a sensor of a surface slope profiler for sub-µrad
11 metrology.

12 The autocollimator was calibrated at the PTB by a direct comparison of the device with a
13 high precision Heidenhain WMT 220 angle comparator [27] as a reference standard [16,17].
14 Figure 2 shows the measurement set-up for the calibration of the DLTP autocollimators at
15 the PTB. The fundamental principle of the used comparator is the subdivision of the circle,
16 representing an error-free natural standard: 2π rad = 360 degrees. In order to ensure the
17 performance of the comparator, different cross- and self-calibration methods have been
18 applied [28-32]. Finally for the comparator, a standard uncertainty [33] of $u = 0.001$ arcsec
19 (5 nrad) is assigned.

20
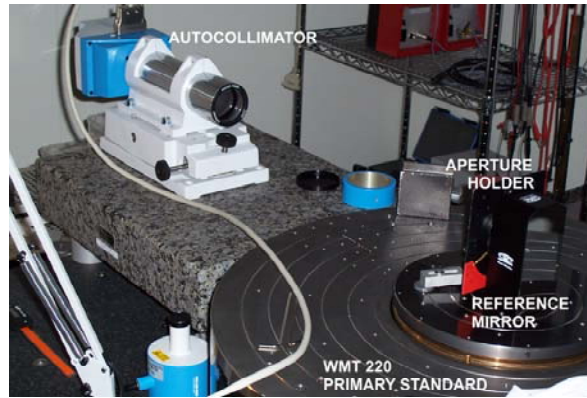
21
22
23 Figure 2: Measurement set-up for the calibration of electronic
24 autocollimators against the PTB angle comparator Heidenhain WMT 220.
25 The autocollimator measures the angle of a plane mirror attached to the
26 comparator's rotor unit. The autocollimator is rotated by 90 degrees to align
27 its main measuring axis for the DLTP application (y-axis) with the
28 comparator's horizontal plane of rotation. The comparator is located in a
29 clean-room laboratory. The lab is kept at a highly stable ambient temperature
30 (ΔT < 0.05 K), a constant laminar air flow (v = 20 cm/s) and very small floor
31 vibrations.

32
33 The calibration data β_{cal} are defined as the angle measurements α_{AC} by the autocollimator
34 minus the angles α_{WMT220} provided by the primary standard:

$$\beta_{cal} = \alpha_{AC} - \alpha_{WMT220}. \tag{1}$$

36 Therefore, to correct a raw angle reading α_{AC} of the autocollimator, the calibration value
37 β_{cal} has to be subtracted from it:

3

$$\alpha_{AC}^{corr} = \alpha_{AC} - \beta_{cal}. \qquad (2)$$

Two different sets of calibrations were performed. The parameters for the first calibration set were optimized for the application of the autocollimator in the DLTP, see Table 1.

Table 1: Autocollimator calibration data set for application of the device in the DLTP set-up.

AC Aperture	Distance to SUT	SUT reflectivity	Axis	Calibration range [arcsec]	Sampling [arcsec]
2.5 mm	550 mm	~100 % (aluminum coating)	X & Y	± 1000	10
			Y	± 10	0.2
			Y	± 1	0.02
	330 mm		X & Y	± 1000	10
			X & Y	± 10	0.2
			Y	± 1	0.02
			Y	-350 ± 10	0.2
			Y	-110 ± 10	0.2

Figure 3 shows two selected calibrations (of the y-axis used for the tangential slope measurement) from this data set.
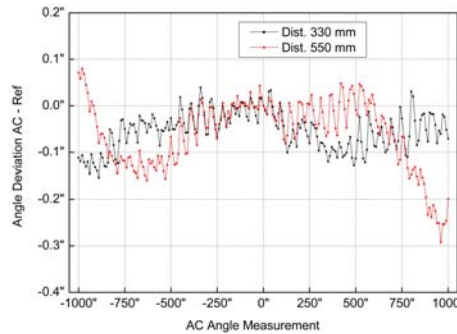
Figure 3: Calibration data for Y-axis of the autocollimator as a function of a difference between slope angle measured with the autocollimator and one provided by the reference standard. The two calibrations correspond to two different baseline distances of 330 mm (the black line and square dots) and 550 mm (the red line and round dots) between the surface under test and the autocollimator. A circular aperture with diameter of 2.5 mm was placed in front of a high reflectance, aluminum coated reference surface. The aperture is precisely centered on the optical axis of the autocollimator. The saw-tooth-like pattern on small angular scales is caused by the aliasing effect discussed in the text.

The calibrations cover an angle range of ±1000 arcsec (±4.85 mrad) with sampling steps of 10 arcsec (49 µrad). The reflecting surface under test, a temperature stable ceramic mirror, coated for high reflectivity, was placed 330 mm and 550 mm from the autocollimator. A circular aperture with a diameter of 2.5 mm was placed directly in the front of the reflecting mirror and, by means of an auxiliary laser pointing device, centered on the optical axis of the autocollimator. This location of the aperture is strongly recommended for deflectometric applications. A standard measurement uncertainty of $u = 0.015$ arcsec (0.073 µrad) is stated [expanded measurement uncertainty $U = 0.03$ arcsec (0.146 µrad) with a coverage factor $k = 2$]. Measurement uncertainties are calculated according to [33,34]. The standard

4

1 measurement uncertainty corresponds to the 68% level of confidence in case of a normal
2 distribution; whereas, the expanded uncertainty with coverage factor $k = 2$ corresponds to
3 the 95% level of confidence [35].

4 The deviations on large angular scales in Fig. 3 are caused by aberrations of the optical
5 components of the autocollimator and errors in their alignment. The saw-tooth-like
6 oscillating pattern on smaller angular scales (Fig. 4) is caused by aliasing as deviations in
7 the autocollimator's angular response with a period of approx. 2.4 arcsec (11.6 µrad) –
8 which corresponds to the 7 µm pixel pitch of the CCD detector – are not properly sampled
9 due to the larger sampling step of 10 arcsec (49 µrad). The stability and precision of our
10 calibration equipment allows for the resolution of these periodic deviations, see Fig. 4.
11 However, it is currently not possible to obtain a calibration over the entire measurement
12 range of the autocollimator which is adequately sampled at all angular scales in a reasonable
13 amount of time. Larger sampling steps have to be used and aliasing effects do occur. In
14 Sec. 4.1, a second type of quasi-periodic angle deviation on an angular scale of approx.
15 60 arcsec (280 µrad) is featured which is caused by internal reflections within the
16 autocollimator itself. Note that the amplitudes of both types of periodic errors are functions
17 of the aperture size and the reflectivity of the surface under test. Unfortunately, due to
18 differing sensitivities to these variables, both error types can not be minimized
19 simultaneously by a well chosen set of parameters.
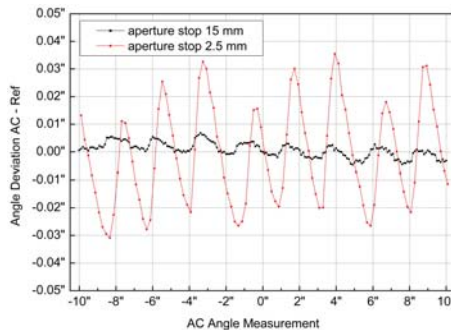
20
21
22 Figure 4: Calibration data (Y-axis of autocollimator) obtained with a
23 sampling of 0.2 arcsec demonstrate periodic deviations in the
24 autocollimator's angular response. The 2.4 arcsec (11.6 µrad) period
25 corresponds to the 7 µm pixel pitch of the CCD detector. Changing the
26 calibration parameters of the SUT reflectivity (from ~ 100% to ~4%) and the
27 aperture diameter [from 2.5 mm (the red line and round dots) to 15 mm (the
28 black line and square dots)] results in reducing the periodic deviations by a
29 factor of >10.

30
31 The parameters for the second calibration set were optimized for an application of the
32 autocollimator as a traceable secondary standard in the Universal Test Mirror (UTM)
33 calibration device [24], see Table 2.

34 Table 2: Autocollimator calibration data with uncoated Zerodur SUT set for
35 application of the device in the UTM set-up.

AC aperture	Distance to SUT	SUT reflectivity	Axis	Calibration range [arcsec]	Sampling [arcsec]
15 mm	250 mm	4 %	X & Y	± 1000	10
			Y	± 10	0.2

Figure 5 shows a calibration curve of the autocollimator Y-axis over the entire dynamic range of the instrument. It covers an angle range of ±1000 arcsec (±4.85 mrad) with sampling steps of 10 arcsec (49 µrad). As a reference SUT, a temperature stable uncoated ceramic mirror was used. The mirror was placed 250 mm in front of the autocollimator. A circular aperture with a diameter of 15 mm was mounted in front of the reflecting mirror and precisely centered to the optical axis of the autocollimator. Compared to the calibration with the 2.5 mm aperture (Figs. 3 and 4), angle deviations in Fig. 5 on both large and small angular scales are greatly reduced by the appropriate choice of the calibration parameters, the SUT reflectivity and the aperture size. A comparison of the calibration functions with 0.2 arcsec sampling (over a limited range of ±10 arcsec suitable for metrology with a flat mirror) from both data sets shows that the periodic deviations in the autocollimator's angle response (causing a wave-like aliasing pattern) are reduced by a factor of >10. A standard measurement uncertainty of $u = 0.005$ arcsec (0.024 µrad) is stated (expanded measurement uncertainty $U = 0.01$ arcsec (0.049 µrad) with a coverage factor of $k = 2$).
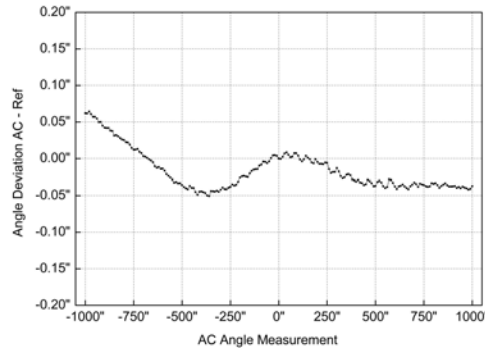
Figure 5: Calibration data (Y-axis of autocollimator) obtained for a SUT (uncoated Zerodur with reflectivity of ~4%) at a distance of 250 mm from the autocollimator. A circular aperture with a diameter of 15 mm was placed in the front of the SUT and centered on the autocollimator's optical axis.

2.2. Pentaprism

In the current version of the DLTP, a bulk pentaprism with a size of 30 mm × 30 mm is used. The inhomogeneity of the glass, flatness of the pentaprism surfaces, and the angle errors of the surfaces would contribute to the systematic error of the DLTP measurements. In order to minimize the systematic error, five pentaprisms made of Homosil 101 were fabricated with the specified surface quality of λ/10, s/d 40/20, angle tolerance 3", and with anti-reflection coating on the two working surface [35]. The pentaprisms were carefully tested with the ZYGO GPI interferometer available at the OML. In the course of the tests, a high quality plane reference mirror with λ/40 shape accuracy (~10 km radius of curvature and about 15 nm peak-to-valley height variation) was measured with a pentaprism placed in the interferometer beam path. The best pentaprism selected this way was mounted on the DLTP optical breadboard and inspected one more time in an arrangement similar to its position in the DLTP. The effective mirror shape, measured with the assembled best pentaprism looked like a smooth cylindrical surface (curved in the tangential direction) with a radius of curvature of approximately 350 m and peak-to-valley variation of about 310 nm [36]. The shape is a result of the optical path perturbation due to the double pass of the light beam through the pentaprism. The quality of the DLTP pentaprism is currently the major limitation of the instrumental performance. In order to solve the problem, we have designed a mirror-based pentaprism that should have significantly higher quality. The corresponding test measurements are in progress.

2.3. Linear translation stage

The DLTP linear translation stage is placed on the optical table with inactivated pneumatic isolation. The stage is designed for translating a carriage with the pentaprism along a ceramic beam over a distance of approximately one meter. The carriage with air-bearing suspension is driven by piezoceramic ultrasonic motors. A linear encoder provides positioning of the carriage with a specified accuracy of ~0.1 microns.

The performance of the stage has been thoroughly investigated with two high precision, temperature stabilized tiltmeters [20]. One tiltmeter was placed on the optical table and another one on the carriage. In this way, a gradual change of tilt of the optical table up to ~15 µrad in response to the changing weight distribution due to carriage translation by 900 mm has been observed. It was also shown that a low spatial frequency imperfection of the ceramic beam profile leads to a change of the carriage tilt of about 12 µrad (peak-to-valley). The shape of the beam and tilt of the table are very repeatable. However, the overall tilt is subject to a drift due to the variation of the ambient temperature.

By monitoring the noise of the tiltmeters, it was found that mis-leveling of the carriage leads to a difference of smoothness of movement in the forward (from left to right) and reverse directions. To minimize the difference, a careful balancing of the carriage, along with alignment of the ceramic beam and loads on the table has been performed. Note that the problems are less significant if a start-stop-measurement mode of DLTP scanning is used.

2.4. Environmental control

The environmental conditions in the lab are supported with an air conditioning system. With the air conditioner on, the overall temperature inside the DLTP plastic enclosed hutch slowly varies by ~120 mK total temperature, decreasing in the late afternoon and night over the course of 12 hours. Due to the air conditioning system's on/off cycles, there is also a much faster periodic fluctuation of the temperature with an amplitude of ~20 mK and a period of ~12 min.

In order to understand the effect of the ambient temperature variation on the measurement performance of the DLTP, a stability test was carried out for approximately 10 hours. In the course of the test, a reference mirror was directly mounted on the stationary carriage. The measurements were started right after the air conditioner was switched on after ~12 hours during which it was switched off. Figure 6 illustrates the result of the test. There is an extremely slow drift of the measured slopes in the tangential (Y) and in the sagittal (X) directions. At the same time, the 12 min periodical temperature variation leads to a periodic variation of the measured angle with an amplitude of ~ 2 µrad (peak-to-valley). Note that due to the rather poor environmental conditions in the OML, the level of random error of the DLTP is about 2 times higher than that of at the HZB/BESSY-II-NOM. At night, the noise level is clearly lower than at the day time.

The observed temperature drift and periodic variation of the DLTP measurements forces us to performed high accuracy measurements with the air conditioner switched off. In this case, the slow drift error related to the diurnal fluctuation of temperature in the lab is suppressed by using an original optimal scanning strategy described in Ref. [21]; see also Sec. 4.2.
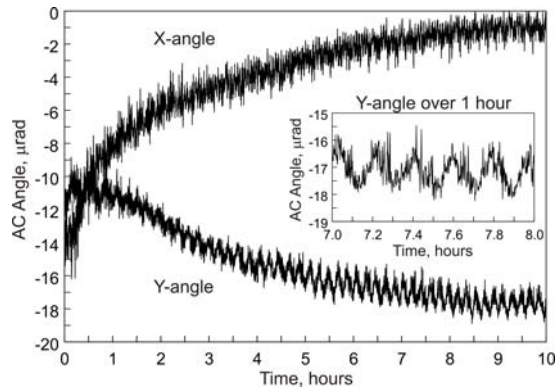
Figure 6: DLTP stability test with a plane reference mirror directly placed on the carriage at the distance of about 200 mm from the autocollimator.

2.5. Motion control and data acquisition system

The DLTP motion control and data acquisition system is based on the NI LabView[TM] platform. This allows to adapt standard ALS beamline control software and, by making relatively simple modifications to the software, to incorporate more efficient measurement methods and techniques.

The system provides two modes of measurement. The on-the-fly mode is used for a faster measurement with a relatively low precision. When high precision measurements with averaging of the autocollimator signal are required, the move-stop-wait-measure-move mode is used. This mode is also useful for suppressing the parasitic effects of the carriage wobbling and wiggling, for example, when precision measurements with a tiltmeter are performed [20]. A trade-off from this is an increase of the measurement time.

In order to carry out measurements after working hours, when the environmental conditions in the lab are most quiet, there is a start delay option. The DLTP data acquisition software also allows tracing a SUT with scanning in two opposite directions, the forward (F) and the reverse (R) directions. The number of scans of a measurement run and a sequence of the scanning directions can be set prior the measurement. We actively use this option in order to run the measurements with a desired optimal scanning strategy for effective suppression of errors due to the instrumental and set-up drifts (Sec. 4.2).

The DLTP software automatically picks up the autocollimator calibration file which is most suitable for the particular experimental arrangement, and applies the calibration to the measured raw data. The raw and the corrected slope data for both tangential and sagittal directions are recorded and saved in a format similar to LTP slope data files. This allows the use of the LTP software to analyze the DLTP data. Additionally, up to ten analog voltage inputs from the Keithley seven-digit multimeter are also gathered in the data file. These inputs can be used for recording of signals from tiltmeters, temperature sensors, etc.

3. Alignment of the DLTP elements

Minimization of the DLTP systematic errors and realization of the advantages of the slope profiler with a movable pentaprism require extremely precise mutual alignment of the DLTP components. Below we provide the details of the used alignment procedure.

3.1. Autocollimator alignment

In order to avoid cross-talk effects in the autocollimator, the AC light beam direction and the axis of the pentaprism translation have to be collinear. The cross-talk would lead, in particular, to a significant sagittal slope variation when a spherical mirror is measured with the DLTP.

To perform the alignment, a collimating iris diaphragm was directly attached to the autocollimator tube and a linear camera [37] was mounted on the DLTP carriage in the front of the pentaprism cube. The camera provided a submicron measurement accuracy of a centroid position of the autocollimator light beam. A proper alignment was obtained by adjusting the AC holder (Fig. 1) to get a stationary position of the light beam centroid over the entire range of motion of the DLTP carriage.

3.2. Pentaprism alignment

In order to precisely align the DLTP pentaprism, we apply a sophisticated procedure developed in Ref. [25]. The procedure is based on a rigorous ray tracing analysis of the measurement errors due to different possible misalignments. As it has been demonstrated with Eq. (4) in Ref. [25], unavoidable errors in the measurement of the tangential slope are induced by changes in the angular orientation of the pentaprism (roll and yaw; we use here the definitions of the corresponding angles given with Fig. 2 of Ref. [25], see Fig. 1) and by changes in the sagittal slope of the surface under test, with both variables interacting. These errors can be minimized by a proper initial angular adjustment of the roll and yaw of the pentaprism relative to the autocollimator (i.e., relative to the coordinate system defined by its optical axis and its two measurements axes, respectively) and of the roll of the SUT. Note that without a sophisticated calibration procedure, it is very difficult to isolate a contribution of the roll angle misalignment to a measured slope profile.

In the first and second orders, a misalignment of the pentaprism pitch angle has no effect ono the slope measurement. Moreover, in order to avoid errors in the autocollimator's angle measurement due to the back reflection from the front and back surfaces of the pentaprism, it is beneficial to make the pitch angle significantly large, such that the reflected beam does not enter the aperture of the autocollimator for the entire range of translation of the pentaprism. Such a deliberate misalignment was introduced into the DLTP.

The pentaprism was optimally aligned to the autocollimator using the pentaprism kinematic base (Fig. 7). As a SUT, we use a high quality plane mirror with diameter of 1 inch. The mirror was mounted on a kinematic stage in a front of the adjustable diaphragm (in the position of the linear camera in Fig. 7). The iris diaphragm was open wide in order to allow the reflection of the autocollimator light beam from the SUT.
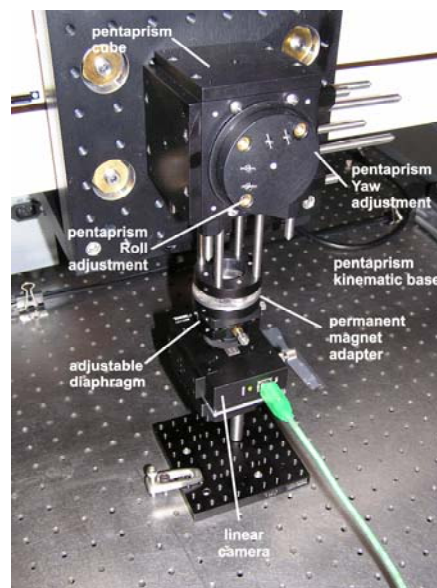
Figure 7: DLTP carriage with the pentaprism cube and adjustable diaphragm (see also text).

1   The first step in the alignment process is to adjust the SUT to its optimal roll angle. This is
2   accomplished by performing what is called the 'yaw test.' To perform the yaw test, the yaw
3   angle of the pentaprism was changed incrementally within a range of approximately ± 0.5
4   mrad and the horizontal (H) and vertical (V) components of the deflection angle measured
5   by the autocollimator were recorded. The theoretical calculations performed in Ref [25]
6   predict a characteristic linear dependence between V and H and when the slope of this line,
7   M_{yaw}, is equal to zero, the SUT is optimally aligned in the roll direction. The value of M_{yaw}
8   is minimized by carrying out an iterative process of adjusting the roll angle of the SUT,
9   performing the yaw test and calculating the slope of V vs. H. The data of the final yaw test,
10   performed after a number of iterations, are shown in Fig. 8. The corresponding V vs. H
11   slope is $M_{yaw} = -0.2$ mrad seen in Fig. 8 as a slope of the best-fit line.
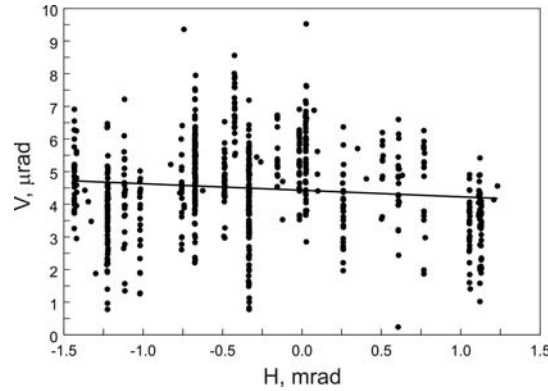
13   Figure 8: Data from the final yaw test.

15   When the SUT roll angle is optimized, the 'roll test' can be performed. This test guides the
16   adjustment of the yaw angle of the pentaprism. The roll test differs from the yaw test in that
17   the roll angle of the pentaprism is changed by approximately ± 0.5 mrad. The theoretical
18   results of Ref. [25] predict a quadratic dependence between V and H. When the minimum of
19   the quadratic fit of the data, H_{roll}, occurs at $H_{roll} = 0$, the yaw angle of the pentaprism is
20   optimally aligned. Again, minimizing H_{roll} involves an iterative process of adjusting the
21   yaw angle of the pentaprism, performing the roll test and calculating H_{roll}. With the DLTP,
22   the roll test was performed a number of times until H_{roll} was minimized to
23     $H_{roll} = -0.262$ mrad. The results from the final roll test are shown in Fig. 9 together with
24   the best-fit second order polynomial (solid line). To minimize linear angle drifts of the
25   experimental set up, the roll and yaw tests were performed in a forward-back sequence.
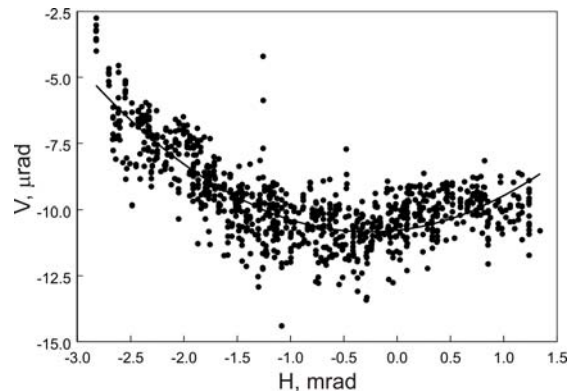
27   Figure 9: Data from the final roll test.

These tests allow the optimal adjustment of the yaw angle of the pentaprism. Finally, adjustment of the roll angle of the pentaprism to its optimal position is a relatively simple task of adjusting the roll angle until the measured H value of the autocollimator reads 0.

With the yaw and roll angles of the pentaprism adjusted appropriately, the pitch angle of the pentaprism is aligned to avoid back reflection for the entire angular range of the autocollimator. It was shown in Ref. [25] that a deviation in the pitch angle of the pentaprism introduces negligible error in the measurements of the deflection angle. This completes the process of aligning the pentaprism.

Finally, the proper position of the adjustable diaphragm with the opening of 2.5 mm diameter was set by symmetrizing the beam profile measured with the linear camera – Fig. 7. In order to enable a large, up to ±10 mm, transfer displacement of an iris diaphragm mounted on a standard ThorLabs Cage System translation stage, a special adapter with permanent magnet holder was designed and fabricated.

4. Measurement procedures and finesses

The calibrations discussed in Sec. 2.1 were carried out at a few fixed baseline distances between the autocollimator and the reflecting surface and allow a significant accounting of the systematic measurement errors of the autocollimator. However, when an autocollimator is used as a profiler sensor, the calibration has a limited performance. As it was shown in Ref. [24] (see also Fig. 3), in the case of a continuously changing baseline distance, errors occur which are not accounted for by the calibrations performed at fixed distances. In order to completely solve the problem, a more sophisticated calibration method and dedicated equipment have to be developed. In Sec. 4.1, we describe an experimental method that allows us to improve the performance of the reliability of the DLTP measurements without an additional calibration.

The periodic variation of temperature due to the switching-on/-off cycle of the lab air conditioner forces us to switch off the air conditioner when performing a precise measurement with the DLTP. With the air conditioner switched off, a slow drift of the room temperature appears with a diurnal peak-to-value variation up to a few degrees C. The drift leads to a DLTP diurnal drift of up to 50 µrad (peak-to-value). At first glance, we have a deadlocked situation. However, as it was suggested in Ref. [21], the negative effect of temperature drift can be significantly suppressed by averaging over slope traces obtained via an appropriate strategy of scanning along a mirror under test – Sec. 4.2.

4.1. Suppression of periodic variations of AC calibration.

The influence of periodic systematic contributions to the angle errors of the electronic autocollimator is significantly reduced by averaging over slope traces measured with a controlled difference in the tangential tilt of the SUT. In the simplest case of averaging only two traces, the difference should be equal to half of the period of the oscillation in the calibration of the autocollimator. The effectiveness of the method is demonstrated below with DLTP measurements with a super polished 15 m spherical test mirror with dimensions of 150 mm (length) × 25 mm (width) × 50 mm (height). The test mirror was provided by InSync Inc [38] as a possible curved surface reference.

Figure 10a reproduces a residual slope trace of the mirror surface measured with the DLTP. The trace is the average of 8 forward (F) and reverse (R) scans performed according to the scanning sequence of {F-R-R-F-R-F-F-R}, optimal to suppress a third order polynomial drift (see Sec. 4.2). In the course of the measurement, the OML air conditioner was switched off. The best-fit spherical shape with a radius of curvature of 14.978 m is subtracted. The clearly seen oscillations with a period, expressed in angular units, of about 280 µrad are due to the instrument's systematic error, caused by the internal reflections within the

1 autocollimator. The oscillations are expected to be most prominent at a combination of a
2 large aperture and high SUT reflectivity. However, the internal reflections still affect the
3 measurement performed with a rather small aperture of 2.5 mm. Note that a similar
4 oscillation with a period of ~295 µrad are observed with the NOM autocollimator.
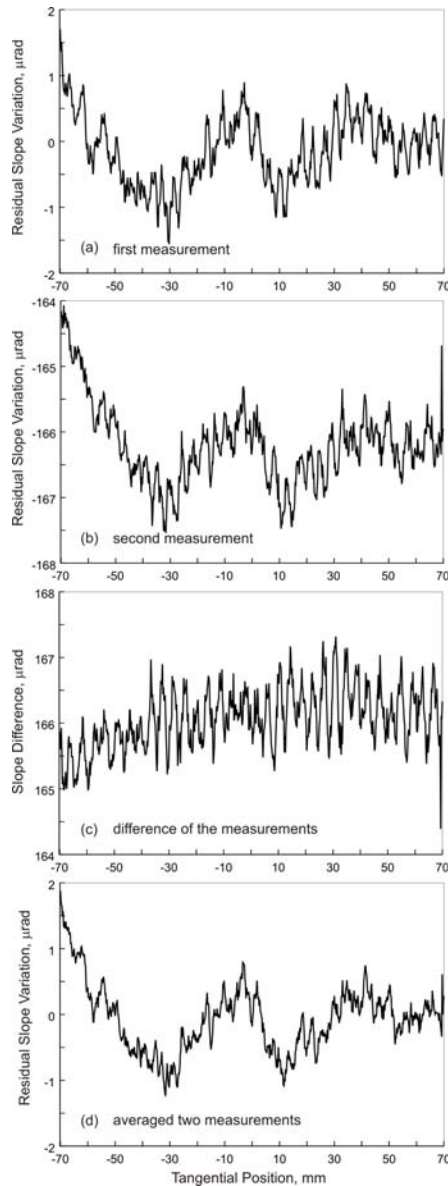
5

6   Figure 10: DLTP measurements of the 15 m spherical test mirror. (a) The residual
7   slope trace measured in the first run of {F-R-R-F-R-F-F-R} scans. The best-fit
8   spherical shape with a radius of curvature of 14.977 m is subtracted. (b) DLTP
9   measurement similar to that of (a) but with the mirror tilted in the tangential
10   direction by 144 µrad. (c) Difference of the measurements shown in plots (a) and
11   (b). This slope trace can be thought of as twice the self calibration function of the
12   instrument. (d) Residual slope variation trace averaged over the measurements
13   presented in plots (a) and (b). The systematic oscillation is significantly suppressed
14   and the resulting trace is a more reliable measure for the surface slope variation.

15 In order to verify that the slope oscillations in Fig. 10a are due to the AC systematic error
16 rather than due to the test mirror surface topography, the same trace was re-measured with a
17 relative tilt of the mirror equal to half of the period of the oscillation, Fig.10b. After the

12

1 measurement, the averaged tilt value of about 144 µrad was verified by subtracting the two
2 measurements. The difference of the measurements is shown in Fig. 10c. This oscillating
3 slope trace can be thought of as twice the self calibration function of the instrument. By
4 using the measured exact curvature of the test mirror, the difference slope trace in Fig. 10c
5 can be converted to the DLTP calibration function with an abscissa in angular units. This
6 calibration can be used as a self calibration of the instrument for the measurement of other
7 mirrors.

8 The systematic oscillations are significantly suppressed in the resulting trace, Fig. 10d,
9 obtained by averaging over the measurements presented in Fig. 10a and Fig. 10b. Note that
10 in order to account for the error with the used calibration method, one has to adequately
11 sample the AC dynamic range which is difficult due to limits on the calibration time.

12 The suggested method does not suppress systematic errors with lower spatial frequencies or
13 an aperiodic error. The profiler systematic errors can be reliably reduced with a
14 sophisticated calibration of the slope profiler as one suggested in Ref. [24] and based on a
15 Universal Test Mirror (UMT) that is to be specially designed for calibration of errors due to
16 the continuously changing baseline distance. Work to develop a UTM system is in progress
17 as a collaborative project of the ALS, BESSY, and PTB metrology teams.

18 Note that by averaging the measurements with a SUT tilted at different angles, one can
19 suppress some instrumental systematic errors at lower spatial frequencies [23].

4.2. Optimal measurement strategies

21 Generally, the measured value, $\Phi_{MES}(x_i)$, of the of slope, $\Phi(x_i)$, are affected by random
22 errors, $R(x_i)$, systematic error, $S(\Phi(x_i),x_i)$, which can depend on the absolute value of the
23 slope, and drift $D(x_i(t))$:

$$\Phi_{MES}(x_i) = \Phi(x_i) + R(x_i) + S(\Phi(x_i),x_i) + D(x_i(t)), \qquad (3)$$

25 where x_i is the measured point position, $i = \{0,..,I-1\}$, and I is the total number of
26 measured points. The contribution of random errors can, in principle, be made as small as
27 required simply by averaging multiple sequential scans $\Phi_{MES,s}(x_i)$, $s = 1,…,S$, carried out
28 at the same experimental conditions:

$$\left\langle \Phi_{MES}(x_i) \right\rangle_S = \frac{1}{S}\sum_{s=1}^{S}\Phi_{MES,s}(x_i) = \Phi(x_i) + \frac{1}{\sqrt{S}}R(x_i) + S(\Phi(x_i),x_i) + \left\langle D(x_i(t)) \right\rangle_S . \qquad (4)$$

30 The systematic error is a part of the measurement error that is systematically reproduced in
31 the sequential scans and, therefore, cannot be suppressed by averaging over repeated
32 measurements. As we have discussed above, precision testing and calibration of the
33 instrument is, practically, the only reliable way to totally eliminate the systematic errors.

34 The drift errors are caused by a relatively slow variation of the experimental conditions such
35 as temperature, humidity, etc. Unlike a random noise, the error contribution of a drift cannot
36 be averaged out using multiple scans identically carried out over a reasonable time. In
37 contrast to systematic errors, drifts are usually not stable enough for accounting via a precise
38 calibration.

39 In Ref. [21], it was shown that an optimal scanning strategy applied to the measurements
40 with a slope measuring profiler allows a significant reduction of systematic effects related to
41 the temporal drifts of the experimental setup and the measuring instrument. Below, we
42 briefly review the method in connection with the DLTP measurements.

1 The idea of the method is to introduce an anti-correlation between the measured angle and
2 the drift error via reversing the sign of the surface slope angle by an appropriate pattern for
3 the sequential scans:

$$\Phi_{MES,s}(x_i) = r_s \Phi(x_i) + D(x_i(t_{i,s})), \tag{5}$$

4

5 where $\{r_s\}$ is a sequence of +1s and -1s, $r_s = +1$ if the s-th scan is performed without
6 reversing, and $r_s = -1$ if the s-th scan is performed with reversing. After averaging over S
7 total number of scans, the measured angle is:

$$\left\langle \Phi_{MES}(x_i)\right\rangle_S = \frac{1}{S}\sum_{s=1}^{S} r_s \Phi_{MES,s}(x_i)$$

8

$$= \hat{\Phi}(x_i) + \frac{1}{S}\sum_{s=1}^{S} r_s D(i\cdot\delta t + (s-1)\cdot\Delta t), \tag{6}$$

9 where δt is a duration of a single measurement (including the time for moving between the
10 sequential points, resting in the position for stabilization, and measuring) and $\Delta t = \delta t \cdot I$ is
11 the duration of a single scan. Assuming that the drift is slow and can be presented as a
12 MacLaurin polynomial series:

$$D(t) = \sum_{n=0} d_n t^n, \tag{7}$$

13

14 a general identity for finding an optimal sequence $\{r_s\}$, which allows to zero out the
15 contribution of the drift terms in (7) up to the n-th polynomial, is derived from (6) [21]:

$$\sum_{s=1}^{S=2^n} r_s(s-1)^{n-k} \equiv 0, \quad 1 \le k \le n \tag{8}$$

16

17 A recursion rule for finding $\{r_s\}$ as well as a general solution of Eq. (8) are provided in [21].
18 The sequences that suppress a linear, first order, drift are obvious:

$$\{r_s^+\} = \{+1,-1\} \quad \text{and} \quad \{r_s^-\} = (-1)\{r_s^+\} = \{-1,+1\}. \tag{9}$$

19

20 The recursion rule [21] provides a simple method to construct solutions for the $(n+1)$-th
21 order polynomial based on the know solutions for the n-th polynomial:

$$\{r_s^+(n+1)\} = \{r_s^+(n), r_s^-(n)\}, \quad \{r_s^-(n+1)\} = (-1)\{r_s^+(n+1)\} \tag{10}$$

22

23 The recursion rule (10) means that an optimal strategy $\{r_s^+(n+1)\}$ for the suppression of a
24 polynomial drift of $(n+1)$-th order is obtained by stitching the solutions $\{r_s^+(n)\}$ and
25 $\{r_s^-(n)\}$ found for the previous order. It allows constructing the optimal scanning strategies
26 to suppress a slow drift up to any desired order of the MacLaurin series of the temporal
27 dependence of the drift. For example, the reversal sequences

$$\{r_s^+(2)\} = \{-1,+1,+1,-1\} \quad \text{and}$$

28

$$\{r_s^-(2)\} = \{+1,-1,-1,+1\} \tag{11}$$

29 are optimal for suppression of drift characterized by a second order polynomial. Effective
30 suppression of the drift described by a third order polynomial would require the use of one
31 of these sequences of 8 scans:

$$\{r_s^+(3)\} = \{+1,-1,-1,+1,-1,+1,+1,-1\} \quad \text{and}$$

32

$$\{r_s^-(3)\} = \{-1,+1,+1,-1,+1,-1,-1,+1\}. \tag{12}$$

The sign of the surface slope angle can be reversed by reversing the DLTP scanning direction and simultaneously flipping the orientation of the SUT [21]. Unfortunately, the current DLTP set-up does not allow to automatically flip the SUT orientation. Therefore, we cannot fully realize the advantages of the described method. However, a significant (rather than the total) suppression of drift errors can still be obtained by solely reversing the DLTP scanning direction according to the same optimal reversing sequences [21]. We use this option in combination with a manual flipping of the SUT orientation applied between the optimal scanning strategy runs. The flipping also allows for additional suppression of a systematic error even with respect to the flipping [39] (see also Sec. 5).

5. DLTP measurement performance

In this section, the sub-microradian performance of the DLTP is demonstrated via a number of measurements with high quality reference mirrors: a super polished plane silicon grating substrate [40] (Sec. 5.1), a curved reference optic with radius of curvature of 1280 meters [41,42] (Sec. 5.2), and a significantly more curved 15-meter spherical test mirror [38]. The DLTP measurements are compared to the metrology of the same optics performed with the upgraded ALS LTP-II and the HZB/BESSY-II NOM (in the case of the 1280-m sphere).

5.1. DLTP metrology of a plane SUT

A plane diffraction grating substrate made of a single crystal Si [40] and super polished was measured with the DLTP and with the upgraded ALS LTP-II [23], providing cross-comparison of the instruments. The substrate figure is specified for a slope error of < 0.3 µrad (rms) over the length of the clear aperture of 180 mm. The measurements were made with the lab air conditioner switched off and with applying the experimental finesses and optimal scanning strategies as discussed in Sec. 4.2. Figure 11 presents the results of the measurements. The total number of scans averaged to get each trace is 16. This includes two runs with flipping the SUT orientation. Each run consisted of 8 scans, see (12), with reversal of the scanning direction.

From Fig. 11a, the slope variation is 0.18 µrad (rms) and 0.15 µrad (rms) as measured with the DLTP and the LTP, respectively. The difference of the measurements is shown in Fig. 11b. The rms variation of the difference is 0.13 µrad. It includes a systematic discrepancy of the instruments that is fitted with the 3rd order polynomial (the dashed line). The peak-to-valley magnitude of the discrepancy is about 0.2 µrad. The residual random noise of the measurements is about 0.07 µrad (rms). Note that the systematic errors of the DLTP and the LTP-II, because of their different constructions, have to be significantly different. Therefore, by averaging the measurements performed with the instruments, one can get even more reliable metrology data with a contribution of the systematic errors smaller by a factor of about two.
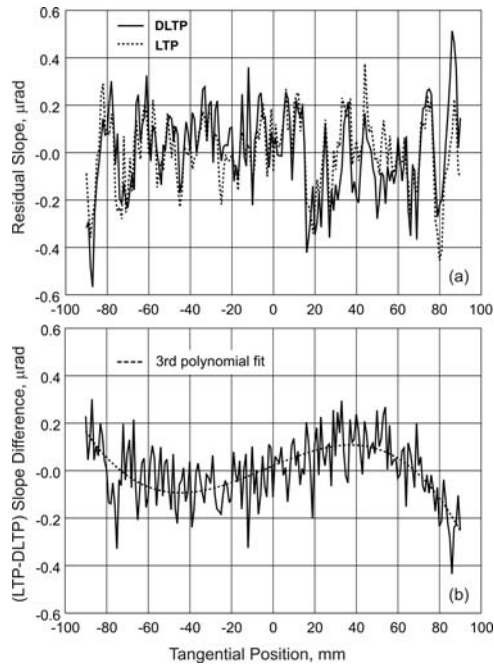
Figure 11: (a) Metrology of a super high quality flat mirror performed with the DLTP (the solid line) and the ALS LTP-II (the dashed trace). (b) The difference of the measurements in (a).

5.2. DLTP measurements with a 1280 m spherical mirror

Next, the DLTP measurements of a high quality 1280 m radius spherically shaped uncoated Si reference mirror are presented. The reference mirror, labeled S3, belongs to the SOLEIL synchrotron, and is used for intensive Round Robin cross-comparisons of slope measuring profilers around the world [41,42].

The S3 reference mirror is specified [43] to have a 1280 m radius spherical shape with residual slope error of 0.5 µrad (rms) over a clear aperture of 110 mm. For Round Robin cross-comparison, a slope trace with 1-mm increments should be measured with the mirror oriented face-up and supported by balls or cylinders at the Bessel points separated by 67 mm. Unfortunately in our case, the last condition was not fulfilled and the mirror was rested on the top aluminum plate of a lab jack with a clean tissue between the optic and the plate. This could slightly effect the final result on the radius of curvature.

The run strategy used with the S3 reference mirror included all the experimental methods and precautions discussed in Sec. 4. In the course of the measurement, the OML air conditioner was switched off. The measurement consisted of six runs in total; no special selection of the runs to be averaged was made – Table 3. Three runs were carried out at the direct orientation of the mirror, and three runs with the reversed mirror orientation. For each run of the total six, the mirror was realigned to have a different tangential tilt that appears in a corresponding slope trace as an offset. We should also mention that because of the drift of the profiler set-up, the tilt offset is changing from scan to scan composing a run. Ironically, we expect this circumstance to be helpful for better averaging of the DLTP systematic errors.

16

Table 3: Experimental parameters of the DLTP measurement with the S3 reference mirror. The tilt offsets were calculated by averaging over all slope angles of the corresponding trace of the run. The gaps in the file numbers listed in Table 3 appear because a short run, usually of 2 scans, was performed in some cases to verify the desired tilt angle after a realignment of the mirror.

| Run Number	Mirror Orientation	Tangential Tilt, µrad	Sagittal Tilt, µrad
#199	direct	-29.9	-0.2
#200	direct	-42.3	+18.5
#201	direct	-56.0	+4.2
#203	reversed	+210.9	-9.2
#205	reversed	+90.7	-2.6
#207	reversed	-7.7	+2.8

Each run listed in Table 3 consists of 16 scans in total, including four consequent series of F-B-B-F scans. The runs listed in Table 1 were usually started at ~6 PM and finished by ~10 AM of the next day.

Figure 12 presents the DLTP and NOM measurements with the S3 reference mirror. The residual tangential slope trace obtained with the DLTP (solid line in Fig. 12a) is a result of averaging over the six runs listed in Table 3 and subtracting the best-fit spherical surface shape with a radius of curvature of 1287.5 m.

An excellent coincidence of the measurements performed with the ALS DLTP and HZB/BESSY-II NOM is clearly seen in Fig. 12b, where the difference of the NOM and DLTP measurements is shown. By and large, the difference of the measurements does not exceed 0.1 µrad (peak-to-valley); the rms variation of the difference is 86 nrad.
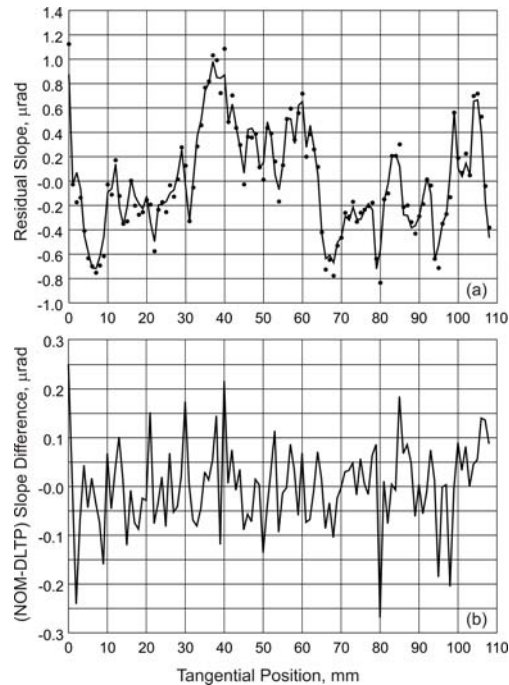
Figure 12: (a) The residual slope variation of the S3 reference mirror measured with the DLTP (solid line) and NOM (solid dots). The best-fit spherical surface shape with a radius of curvature of 1287.5 m (DLTP data) and 1280.4 (NOM data) was subtracted. (b) Difference of the measurements in (a).

5.3. Measurements with 15 m mirror metrology and comparison with the LTP

The DLTP performance with significantly curved x-ray optics was verified by measuring a 15 meter spherical test mirror [38]. The strong mirror curvature allows testing the DLTP over the entire dynamic range of the AC, which is ±4.8 mrad. The result of two DLTP runs with the mirror in the same orientation has been discussed in Sec. 4.1; see Fig. 10. In addition to the measurements shown in Fig. 10, two more similar runs but with a flipped orientation of the mirror were carried out. The resulting slope trace averaged over all four runs is shown in Fig. 13a. The best-fit spherical surface shape with a radius of curvature of 14.977 m is subtracted. Figure 13b presents the difference of the measurements performed at two opposite orientations of the mirror. The difference is a systematic error of the DLTP measurement that is eliminated by averaging over measurements with different orientations of the mirror. Probably, the major contribution to the systematic error depicted in Fig. 13b is due to the imperfection of the DLTP pentaprism (see Sec. 3.2). The observed increase of the systematic error to the ends of the mirror can partially relate to the limited reliability of the calibration of the AC performed at the fixed distance.

The random noise of the DLTP in the course of the measurements with the 15 m test mirror can be estimated as a difference between a single scan trace and a trace, such as a run trace shown in Fig. 10d, averaged over a large number of repeated scans. The residual rms slope variation of 0.2 µrad observed for a single scan seems to be a very exiting result if one takes into account that in the course of measurements the OML air conditioning was switched off.

Figure 14 compares the results of the DLTP and LTP measurements of the 15-m spherical test mirror. The DLTP trace in Fig. 14a the same as one in Fig. 13a. However in order to match the arrangement of the LTP measurements, each two sequential points of the trace are averaged and the result is shown over the tangential positions of ±40 mm with an increment of 0.4 mm.
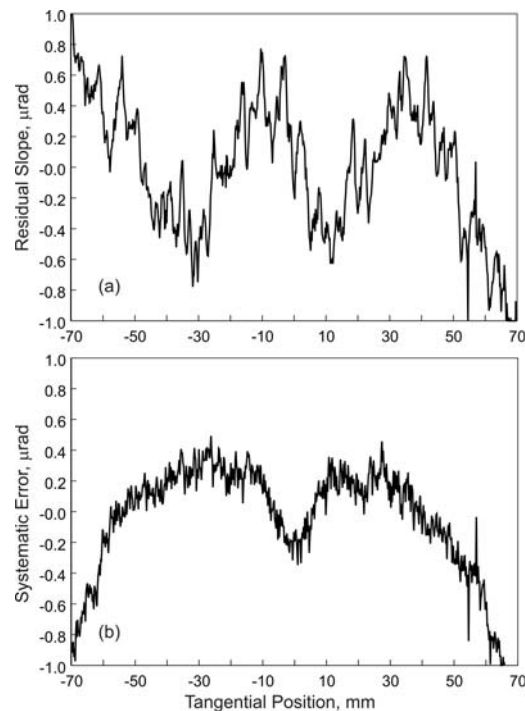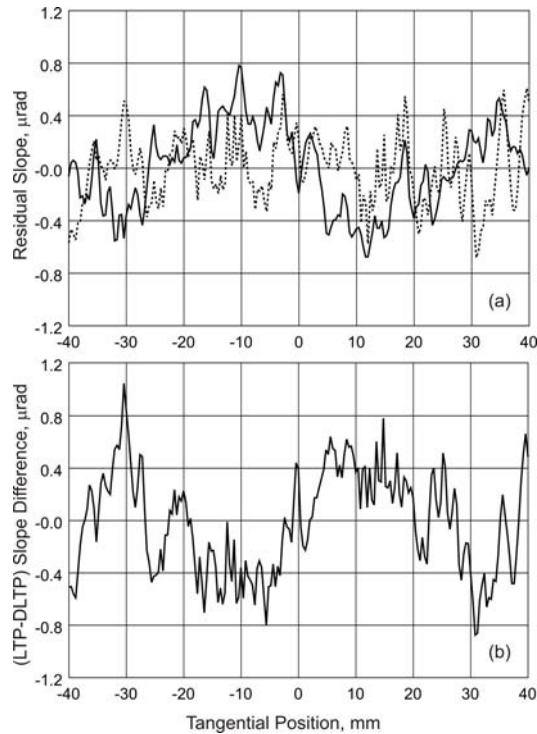

Figure 13: (a) DLTP metrology of a 15-m spherical test mirror [38]. The spherical shape with the measured radius of curvature of 14.977 m is subtracted and the residual slope variation is shown. (b) DLTP systematic error removed by averaging the measurements performed with flipping of the mirror orientation (see text).

18

Figure 14: (a) Residual slope variation of the 15-m spherical test mirror [38] as measured with the DLTP and the upgraded ALS LTP-II. The spherical shape with the measured radius of curvature of 14.977 m (DLTP) and 15.072 is subtracted and the residual slope variation is shown. (b) Difference of the measurements in (a). (see text).

The residual tangential slope trace measured with the LTP (dashed line in Fig. 14a) is a result of averaging over the 4 runs of 8 optimal scans each. Two first runs were performed with the same orientation of the mirror, but with the sagittal tilts being different by ~100 µrad. The second two runs were performed with a flipped orientation of the mirror. The best-fit spherical surface shape with a radius of curvature of 15.072 m is subtracted.

The difference of the DLTP and the LTP measurements is shown in Fig. 14b. The rms variation of the difference is about 0.36 µrad. It is mostly due to a systematic slope variation, which can be fitted with a 5th order polynomial function with a peak-to-valley magnitude of about ±0.4 µrad. Note that with a similar 15-m spherical SUT, the systematic errors of the LTP, estimated by comparing with the corresponding NOM measurements, is less than 0.25 µrad [23]. Therefore, the systematic variation in Fig. 14b is mostly due to the limitations of the DLTP calibration.

6. Discussion and Conclusions

The high performance of the ALS DLTP has been confirmed via a cross-comparison with metrology performed with the upgraded ALS LTP-II and the HZB/BESSY-II NOM. It has been shown that the DLTP provides an absolute accuracy of <0.1 µrad with plane and slightly curved x-ray optics, and <0.4 µrad with significantly curved optics. The demonstrated performance of the DLTP is based on the initial precision calibration of the autocollimator. The original strategy of measurement and sophisticated experimental finesses developed and implemented at the ALS OML allow for an efficient suppression of the instrumental systematic and drift errors. However, if the same strategy and finesses are applied while measuring with the NOM, the result is expected to be significantly better. This is mainly because of the stable massive granite table and extremely quiet

environmental conditions provided with a special climatic system and multi-room arrangement of the HZB/BESSY-II optical metrology laboratory.

The current performance of the DLTP set-up is limited by a number of systematic errors. The systematic error due to the finite quality of the bulk pentaprism can be substantially reduced by using a pentaprism made of precisely adjusted high quality plane mirrors as was done at the NOM. The corresponding work is in progress. The limitation related to the AC calibration at a fixed distance between the AC and the SUT, can be overcome with a sophisticated *in-situ* calibration of the profiler. A first set up of a vertical angle comparator has been realized at the HZB/BESSY-II [44,45] and it has been shown to be reasonable in its use for the additional calibration of the NOM. In the course of the calibration, a 5th order polynomial correction has been introduced (compare with the DLTP systematic error shown in Fig. 14b). A more sophisticated design, the Universal Test Mirror (UTM), was proposed recently [24], and is under development by a cooperation of the ALS, HZB/BESSY-II and the PTB.

In order to fully realize the advantages of the suppression of the instrumental drift error with the optimal scanning strategies derived in Ref. [21], a Huber-stage-based rotation system for automatic flipping the SUT is being developed.

One of the most important developments that are still expected to be realized at the ALS OML is improvement of the laboratory environmental conditions and lab arrangement.

Replacement of the existing optical table with a table similar to one used for the NOM set-up would provide an opportunity for two dimensional slope mapping of high quality x-ray optics. The current performance of the two dimensional metrology with the NOM has allowed the use of metrology data as input data for a deterministic shape optimization of plane and curved optical elements [46,47].

We believe that by realizing the listed improvements an absolute slope measuring performance below 0.1 µrad can be achieved.

Acknowledgements

Disclaimer

Certain commercial equipment, instruments, or materials are identified in this document. Such identification does not imply recommendation or endorsement by the US Department of Energy, LBNL, or ALS, nor does it imply that the products identified are necessarily the best available for the purpose.

References:

[1] L. Assoufid, O. Hignette, M. Howells, S. Irick, H. Lammert, P. Takacs, "*Future metrology needs for synchrotron radiation grazing-incidence optics,*" Nucl. Instrum. and Meth. in Phys. Research A **467-468**, 267-70 (2001).

[2] P. Z. Takacs, "X-Ray Mirror Metrology," in Handbook of Optics, 3rd edition, M. Bass, ed., vol. V, ch. 46 (in press).

[3] E. Debler, K. Zander, „*Ebenheitsmessung an optischen Planflächen mit Autokollimationsfernrohr und Pentagonprisma*, PTB Mitteilungen Forschen + Prüfen, Amts und Mitteilungsblatt der Physikalisch Technischen Bundesanstalt, Braunschweig und Berlin, 1979, pp. 339-349.

[4] Frank Siewert, Tino Noll, Thomas Schlegel, Thomas Zeschke, and Heiner Lammert, "*The Nanometer Optical Component Measuring machine: a new Sub-nm Topography Measuring Device for X-ray Optics at BESSY*," AIP Conference Proceedings 705, American Institute of Physics, Mellville, NY, 2004, pp. 847-850.

[5] H. Lammert, T. Noll, T. Schlegel, F. Siewert, T. Zeschke, „*Optisches Messverfahren und Präzisionsmessmaschine zur Ermittlung von Idealformabweichungen technisch polierter Oberflächen*," Patent No.: DE 103 03 659 (28 July 2005).

[6] F. Siewert, H. Lammert, T. Zeschke, "*The Nanometer Optical Component Measuring Machine*;" in: Modern Developments in X-ray and Neutron Optics, Springer 2008.

[7] R.D. Geckeler, I. Weingärtner, "*Sub-nm topography measurement by deflectometry: flatness standard and wafer nanotopography*," Proc. of SPIE, 4779, Bellingham, WA, 2002, pp. 1-12.

[8] R.D. Geckeler, "*Error minimization in high-accuracy scanning deflectometry*," Proc. SPIE 6293 (2006) 62930O 1-12.

[9] Ralf D. Geckeler, "*ESAD Shearing Deflectometry: Potentials for Synchrotron Beamline Metrology*," Proc. of SPIE, 6317, Bellingham, WA, 2006.

[10] K. von Bieren, "*Pencil beam interferometer for aspherical optical surfaces*," Proc. SPIE 343, 101-108 (1982).

[11] K. von Bieren, Appl. Opt. 22, 2109 (1983).

[12] P. Takacs, S. N. Qian and J. Colbert, "*Design of a long trace surface profiler*," Proc. of SPIE, 749, Bellingham, WA, 1987, pp. 59-64.

[13] P. Takacs, S. N. Qian, "*Surface Profiling interferometer*," US patent No.U4884697, Dec. 5, 1989.

[14] Shinan Qian, Werner Jark, Peter Z. Takacs, "*The penta-prism LTP: A long-trace-profiler with stationary optical head and moving penta prism*," Rev. Sci. Instrum. 66 (3), 2562-25691(995).

[15] R. D. Geckeler, A. Just, M. Krause, V.V. Yashchuk, "*Autocollimator for Deflectometry: Current Status and Future Progress,*" Nucl. Instr. and Meth. A [current issue].

[16] R.D. Geckeler, I. Weingärtner, A. Just, R. Probst, "*Use and traceable calibration of autocollimators for ultra-precise measurement of slope and topography*," Proc. of SPIE, Vol. 4401, Bellingham, WA, 2001, pp. 184-195.

[17] A. Just, M. Krause, R. Probst, and R. Wittekopf, "*Calibration of high-resolution electronic autocollimators against an angle comparator*," Metrologia **40,** 288-294 (2003)**.**

[18] Yashchuk, V. V., "*Positioning errors of pencil-beam interferometers for long-trace profilers,*" Proc. SPIE 6317, 63170A-12 (2006).

[19] Kirschman, J. L., Smith, B. V., Domning, E. E., Irick, S. C., MacDowell, A. A., McKinney, W. R., Morrison, G. Y., Smith, B. V., Warwick, T., and Yashchuk, V. V., "*Flat-Field Calibration of CCD Detector for Long Trace Profilers,*" Proc. SPIE 6317, 67040J-11 (2007).

[20] Kirschman, J. L., Domning, E. E., Morrison, G. Y., Smith, B. V., Yashchuk, V. V., "*Precision Tiltmeter as a Reference for Slope Measuring Instruments,*" Proc. SPIE **6317**, 670409-12 (2007).

[21] V. V. Yashchuk, "*Optimal Measurement Strategies for Effective Suppression of Drift Errors*," Rev. Sci. Instrum. (in press).

[22] Irick, S. C., McKinney, W. R., Lunt, D. L., Takacs, P. Z., "*Using a straightness reference in obtaining more accurate surface profiles from a long trace profiler (for synchrotron optics),*" Rev. Sci. Instrum. **63**(1), 1436-8 (1992).

[23] J. L. Kirschman, E. E. Domning, W. R. McKinney, G. Y. Morrison, B. V. Smith, and V. V. Yashchuk, "*Performance of the upgraded LTP-II at the ALS Optical Metrology Laboratory,*" Proc. SPIE **7077**, 7077-10/1-12 (2008).

[24] V. V. Yashchuk, W. R. McKinney, T. Warwick, T. Noll, F. Siewert, T. Zeschke, and R. D. Geckeler, "*Proposal for a Universal Test Mirror for Characterization of Slope Measuring Instruments,*" Proc. SPIE **6704**, 67040A/1-12 (2007).

[25] R. D. Geckeler, **"***Optimal use of pentaprisms in highly accurate deflectometric scanning,*" Measurement and Science Technology **18** (2007) 115-125.

[26] Elcomat 3000, *Möller Wedel Optical*, http://www.moeller-wedel-optical.com.

[27] R. Probst, R. Wittekopf, M. Krause, H. Dangschat, and A. Ernst, "*The new PTB angle comparator,*" Meas. Sci. Technol. 9 (1998), 1059-1066.

[28] P.J. Sim, "*Angle standards and their calibration,*" in Modern Techniques in Metrology, ed. P.L. Hewitt, 102-121 (World Scientific, Singapore, 1984).

[29] A. Ernst, European Patent 0 440 833 B 1 (1994), patentee: Dr. Johannes Heidenhain GmbH.

[30] R. Probst and M. Krause, "*Six nanoradian in 2π radian – A primary standard for angle measurement,*" Proc. 2nd Euspen (2001), 326-329.

[31] R.D. Geckeler, A. Fricke, and C. Elster, "*Calibration of angle encoders using transfer functions,*" Meas. Sci. Technol. **17**(10), 2811-2818 (2006).

[32] T. Masuda T and M. Kajitani, "An automatic calibration system for angular encoders," Precis. Eng. **11** (1989), 95-100.

[33] Guide to the Expression of Uncertainty in Measurement (ISO, Geneva, 1993).

[34] The relevant definitions can be found, e.g., on the NIST website http://physics.nist.gov/cuu/Uncertainty/coverage.html

[35] Part # 60.999 Special Delivery, OWIS GmbH, Germany (through Pacific Laser Equipment, Inc., http://www.plequipment.com/owis.php).

[36] F. Siewert, V.V. Yashchuk, J.L. Kirschmann, G.Y. Morrison, B.V. Smith, "*Initial Alignment and Commissioning of an Autocollimator Based Slope Measuring Profiler at the Advanced Light Source,*" Helmholtz Zentrum Berlin – Annual Report 2008.

[37] We use a ThorLabs camera model LC1-USB with size of a pixel of 7 µm × 200 µm (http://www.thorlabs.com/newgrouppage9.cfm?objectGroup_ID=1300).

[38] InSync, Inc.; http://www.insyncoptics.com/products.html.

[39] W. R. McKinney, S. C. Irick, D. L. Lunt, *"XUV synchrotron optical components for the Advanced Light Source: summary of the requirements and the developmental program,"* Proceedings of the SPIE **1740**, 154-160 (1993).

[40] The plane substrate for a diffraction grating was fabricated by Carl Zeiss Inc. (Germany) for Free Electron Laser at the Linac Coherent Light Source (LCLS, USA).

[41] Rommeveaux A, Thomasset M, Cocco D, Siewert F., *"First report on a European round robin for slope measuring profilers,"* Proceedings of the SPIE **5921** – 592101 (2005).

[42] F. Siewert, L. Assoufid, D. Cocco, O. Hignette, S. Irick, H. Lammert, W. McKinney, H. Ohashi, F. Polack, S. Qian, S. Rah, A. Rommeveaux, V. Schönherr, G. Sostero, P. Takacs, M. Thomasset, K. Yamauchi, V. Yashchuk, T. Zeschke, *"Global high-accuracy inter-comparison of slope measuring instruments,"* AIP Conference on Synchrotron Radiation Instrumentation SRI-2006, III Workshop on Optical Metrology, CD Proceedings (Daegu, South Korea, May 27 - June 03, 2006).

[43] The S3 mirror specification data and the result of Round Robin measurements with the mirror are courtesy of Amparo Rommeveaux.

[44] F. Siewert, *"Calibration: Calibration and Autocalibration,"* 3rd International Workshop on Metrology for X-ray Optics, Daegu, Korea, June 200.

[45] F. Siewert, J. Buchheim, T. Zeschke, *"Characterization and Calibration of 2nd Generation Slope Measuring Profiler,"* [this conference].

[46] F. Siewert, H. Lammert, T. Noll, T. Schlegel, T. Zeschke, T. Hänsel, A. Nickel, A. Schindler, B. Grubert, C. Schlewitt, *"Advanced metrology: an essential support for the surface finishing of high performance x-ray optics,"* in Advances in Metrology for X-Ray and EUV Optics edited by Lahsen Assoufid, Peter Z. Takacs, John S. Taylor, Proc. of SPIE **5921**-01, Bellingham, WA (2005).

[47] A. Schindler, T. Haensel, A. Nickel, H.J. Thomas, H. Lammert, F. Siewert, *"Finishing procedure for high performance synchrotron optics,"* Optical Manufacturing and Testing, Proc. of SPIE **5180**, 64-72, Bellingham, WA (2003)